Available online at www.sciencedirect.com
ScienceDirect
Journal of Power Sources 171 (2007) 610–616
JOURNAL OF POWER SOURCES
www.elsevier.com/locate/jpowsour

Electrochemical impedance investigation of proton exchange membrane fuel cells experienced subzero temperature

Junbo Hou [a,b], Wei Song [a,b], Hongmei Yu [a,*], Yu Fu [a,b], Zhigang Shao [a], Baolian Yi [a]

[a] *Fuel Cell System and Engineering Laboratory, Dalian Institute of Chemical Physics, Chinese Academy of Sciences, 457 Zhongshan Road, Dalian 116023, PR China*
[b] *Graduate School of the Chinese Academy of Sciences, Beijing 100039, PR China*

Received 27 April 2007; received in revised form 29 June 2007; accepted 3 July 2007
Available online 17 July 2007

Abstract

Polarization losses of the fuel cells with different residual water amount frozen at subzero temperature were investigated by electrochemical impedance spectroscopy (EIS) taking into account the ohmic resistance, charge transfer process, and oxygen mass transport. The potential-dependent impedance before and after eight freeze/thaw cycles suggested that the ohmic resistance did not change, while the change of the charge transfer resistance greatly depended on the residual water amount. Among the four cells, the mass transport resistance of the cell with the largest water amount increased significantly even at the small current density region. According to the thin film-flooded agglomerate model, the interfacial charge transfer process and oxygen mass transport within the agglomerate and through the ionomer thin film in the catalyst layer both contributed to the high frequency impedance arc. From the analysis of the Tafel slopes, the mechanism of the oxygen reduction reaction (ORR) was the same after the cells experienced subzero temperature. The agglomerate diffusion changed a little in all cells and the thin film diffusion effect was obvious for the cell with the largest residual water amount. These results indicated that the slower oxygen diffusion within the catalyst layer (CL) was the main contributor for the evident performance loss after eight freeze/thaw cycles.

Keywords: Proton exchange membrane (PEM) fuel cell; Subzero; Electrochemical impedance spectroscopy; Mass transport; Oxygen reduction reaction; Agglomerate

1. Introduction

The cold start of a PEM fuel cell is a complex transient process coupled with water, heat transport and ice formation. At subzero temperature, the electrolyte, i.e. Nafion®, conductivity is low. The generated water due to the *ORR* will freeze once the heat produced is not enough to warm the membrane electrode assembly (MEA) above the freezing temperature. The freezing of the generated water most likely covers the catalyst sites, reduces the three phase boundaries (TPB) and blocks the reactant gas accessing to the reaction sites. The increased polarization will usually lead to a failure cold start. Another concern is fuel cell survivability relating with the freeze/thaw thermal cycles at subzero temperature. The thermal cycle is a main method to investigate the materials durability. Furthermore, the protocol of the fuel cell shut down is a preliminary way to promise a successful cold start.

Recently, based on the experimental data, Wang's group [1–5] made calculations and set up mathematic modeling. Basic understandings and fundamentals of PEM fuel cell cold start process have been thus boosted a step. The fundamental principles of fuel cell freeze related degradation have not been fully understood yet, though the freeze/thaw cycle has been applied to PEM fuel cell [6–9]. As early as 1995, the freeze/thaw cycle were applied to investigate the integrity of the thin-film catalyst layer and membrane assembly by Wilson et al [10]. After 3 freeze/thaw cycles, they found no cell performance decay. Pivovar and coworkers [11] also found no performance degradation after 100 freeze/thaw cycles down to −40 °C. However, a degradation rate of 2.8% at 0.6 V was observed after 4 freeze/thaw cycles (−10 to 80 °C) [12]. The different results likely indicate the fabrication arts of the catalyst layer and MEA will affect the fuel cell survivability at subzero temperature. The MEA is porous and thus has water storage capacity. Moreover, even though there is

* Corresponding author. Tel.: +86 411 84379051; fax: +86 411 84379185.
E-mail address: hmyu@dicp.ac.cn (H. Yu).

0378-7753/$ – see front matter © 2007 Elsevier B.V. All rights reserved.
doi:10.1016/j.jpowsour.2007.07.015

some water in MEA, the volume expansion from ice formation does not change the pore size distribution [9]. This fact induces a relationship of the freeze related degradation with the residual water amount.

The EIS technique proves a good diagnostic tool which is able to separate the responses of the various transport processes occurring simultaneously in PEM fuel cell [13–16]. Generally, the highest-frequency intercept of an impedance spectrum denotes the cell resistance, and the high-frequency region reflects the charge transport in the catalyst layer, whereas the low-frequency region represents mass transport in the gas diffusion layer (GDL), the CL, and the membrane [13]. Useful information can be acquired from the impedance spectroscopy.

In this work, a study of EIS response was conducted for four cells with different residual water amount frozen at −10 °C for 8 freeze/thaw cycles. The cells were also subjected to polarization experiments. By changing the amount of the residual water, the water saturation in the layers of MEA, especially in the CL was adjusted. And thus the freeze degradation was correlated with the residual water amount using the thin film-flooded agglomerate model. The aim of this study was to elucidate fundamentals of the freeze related degradation taking into account the ohmic resistance, the charge transfer process due to ORR, and mass transport phenomena within the CL.

2. Experimental

2.1. GDE, MEA fabrication and cell configuration

The 50 wt.% home-made Pt/C (Vulcan XC-72) catalyst was fabricated by reducing H_2PtCl with HCHO. Toray carbon paper, Nafion® solution and PTFE suspension were used to fabricate the gas diffusion electrodes (GDEs). The carbon/PTFE slurry was brushed on the two sides of the hydrophobicity treatment carbon paper, and then the carbon paper was dried and calcined. Subsequently, the slurry of the Pt/C dispersion was brushed on the smooth carbon paper. After that, the carbon paper with microporous layer and the CL was dried and calcined in flowing nitrogen gas. Finally, Nafion® solution was sprayed on the catalyst layer. The Pt loading was about 0.5 mg cm^{-2} and the Nafion® loading was 0.6–1.2 mg cm^{-2}. Two electrodes with the effective area of 4 cm^2 and a N212 membrane were hot-pressed to form a MEA. Two graphite polar plates used as current collectors were machined with parallel flow channels. The silicon O-ring was used as a seal and the whole cell was tightened by two organic glass end plates and eight bolts. To measure cell temperature, a pore for the thermal couple was drilled on the side of the graphite polar plate. Details can be found in Ref. [17].

2.2. Residual water amount and freeze/thaw process

The cells were firstly experienced conditioning, performance test and electrochemical measurement. Then, they were purged by dry gas to remove water. To obtain different residual water amounts, four different operation processes were applied (Table 1). The three cells C1–C3 were operated at 25 °C with the dry reactant gases fed in, while the cell C4 ran at 60 °C with humidified reactant gases. The inlet O_2 and H_2 relative humidity (RH) were both 100% which was measured using a hygrometer (Vaisala HMT360, Finland). The gaseous water into the cell could be calculated by the following equation:

$$m_{\mathrm{water,in}} = \left(N_{\mathrm{H_2}} t \frac{P^{\mathrm{in}}_{\mathrm{water,anode}}}{P_{\mathrm{anode}} - P^{\mathrm{in}}_{\mathrm{water,anode}}} + N_{\mathrm{O_2}} t \frac{P^{\mathrm{in}}_{\mathrm{water,cathode}}}{P_{\mathrm{cathode}} - P^{\mathrm{in}}_{\mathrm{water,cathode}}} \right) M_{\mathrm{H_2O}} \quad (1)$$

where N_{H_2} and N_{O_2} are the H_2 and O_2 molar flow rates, t the time, F the Faraday's constant, M_{H_2O} the water molecular weight, P_{anode} and $P_{cathode}$ the gas pressures of anode and cathode, respectively, and $P^{in}_{water,anode}$ and $P^{in}_{water,cathode}$ the water partial pressures of the anode and cathode inlets. The generated water amount could be simply calculated by the Faradic law, and the amount of the water out of the cell was measured by weighing the silica gel tubule which was connected to the cell outlets. The electronic balance (Sartorius BS2202S, Germany) had an accuracy of two significant digits after the decimal point. For the one without weight increase, the RH of the outflow was measured. In these cases, the amount of the gaseous water out of the cell with the reactant gas was estimated according to the following equation:

$$m_{\mathrm{water,out}} = \left(N_{\mathrm{H_2}} - \frac{iA}{2F} \right) t \frac{P^{\mathrm{out}}_{\mathrm{water,anode}}}{P_{\mathrm{anode}} - P^{\mathrm{out}}_{\mathrm{water,anode}}} M_{\mathrm{H_2O}} + \left(N_{\mathrm{O_2}} - \frac{iA}{4F} \right) t \frac{P^{\mathrm{out}}_{\mathrm{water,cathode}}}{P_{\mathrm{cathode}} - P^{\mathrm{out}}_{\mathrm{water,cathode}}} M_{\mathrm{H_2O}} \quad (2)$$

where $P^{out}_{water,anode}$ and $P^{out}_{water,cathode}$ are water partial pressures of the anode and cathode outflow, respectively. A is the MEA

Table 1
Operation processes to obtain different residual water amount in cells

	Current (A cm^{-2})	Run time (s)	Flow rates (ml min^{-1})	Generated water (mg)	Water in (mg)	Water out (mg)	Residual water (mg cm^{-2})
C1	0.1	120	10	4.11	–	0.60	0.9
C2	0.4	120	20	16.41	–	0.94	3.9
C3	0.8	240	30	65.63	–	50.61	3.6
C4	0.8	1800	30	440.34	145.88	420	41.6

effective area. The residual water amount in the cell could be estimated by the amount of the generated water minus the amount of the water out of the cell. These results were all summarized in Table 1.

Subsequently, the cell inlets and outlets were sealed and the cell was put into the climate chamber. The cell temperature was kept at −10 °C for 1.5 h. After that, the cell was taken out of the climate chamber after each freeze cycle, and directly warmed by hot air which was supplied by the air condition. When the cell temperature was above 10 °C, the cell was set up at the home-made fuel cell test station. The reactant gases were fed in the cell, and the gas pressure was kept at 0.03 MPa. The out flow rates were constant at 100 ml min^{-1} for O_2 and 40 ml min^{-1} for H_2. Meanwhile, the cell was heated by the cycling water. The cell performance tests were conducted at 60 °C. Each cell was repeated 8 cycles.

2.3. Performance evaluation and electrochemical study

When the cell temperature reached 60 °C, the cell started up at the current density of 0.5 A cm^{-2} and ran at this current density for 20–30 min. And then, the polarization characterization was conducted for three times at the constant out flow rates of 100 ml min^{-1} for O_2 and 40 ml min^{-1} for H_2. The third data was chosen for comparison. For the cell C4, it was not able to start at 0.5 A cm^{-2}, and was operated at 0.3 A cm^{-2}. The cell performance was usually stable in the process of 20–30 min of equilibrium condition. After the cell performance was measured, the KFM2030 impedance meter (Kikusui, Japan) was connected for in situ EIS measurement using Fuelcell-Load&Impedance Meter software (Kikusui, Japan). The perturbation amplitude for the sine signal was 165 mA (peak to peak) over a frequency range of 10 kHz–0.5 Hz. Since the impedance was measured at galvanostatic mode, the cell voltage was adopted from the corresponding value in *i–v* plot. This was confirmed by comparing the cell voltage in *i–v* plot with that during the process of the impedance measurement at the same current density. Considering the fast rate of hydrogen oxidation reaction (HOR) and small effect of water freezing on the anode [7], impedance data reported in the paper were all measured in two-electrode system.

3. Results and discussion

3.1. Performance evaluation

Fig. 1 shows the performance of the four cells with different water amount frozen at −10 °C for 8 cycles. Comparing the initial cell performance, there is a little difference between voltages in the current density region of 0–1 A cm^{-2} for C1, as shown in Fig. 1a. Increasing the residual water amount makes the performance loss more evident, as shown in Fig. 1b–d. With 3.9 mg cm^{-2} water amount, the cell performance degrades from 0.593 to 0.516 V at 1 A cm^{-2}, while performance loss is from 0.598 to 0.503 V for C3 with 3.6 mg cm^{-2}. For the biggest water amount, the cell is unable to run at 0.5 A cm^{-2}.

The semi-empirical equation as Eq. (3) is used to fit the *i–V* plots in the region of activation and ohmic polarization [18]:

$$E = E_0 - b \log i - Ri \tag{3}$$

where

$$E_0 = E_r + b \log i_0 \tag{4}$$

E_r is the reversible potential, b the Tafel slope, i_0 the exchange current density for the oxygen reduction and R consists of material bulk resistance, interfacial contact resistance and contribution from the mass transport limitation within the catalyst layer. Those parameters can be obtained by non-linear least square fit of the polarization plot and are summarized as well as the cell voltages at 10 mA in Table 2.

3.2. EIS general pattern and ohmic resistance change

The transport processes greatly depend on the overpotential at the steady state [13,14]. The EIS experiment is thus conducted at different cathode potentials, and the typical in situ impedance spectra at different cathode potentials are shown in Fig. 2. The cathode potential is *iR*-corrected cell voltage. From Fig. 2a and b, when the overpotential increases, the arc diameter decreases, which reflects the increasing driving force of the ORR process.

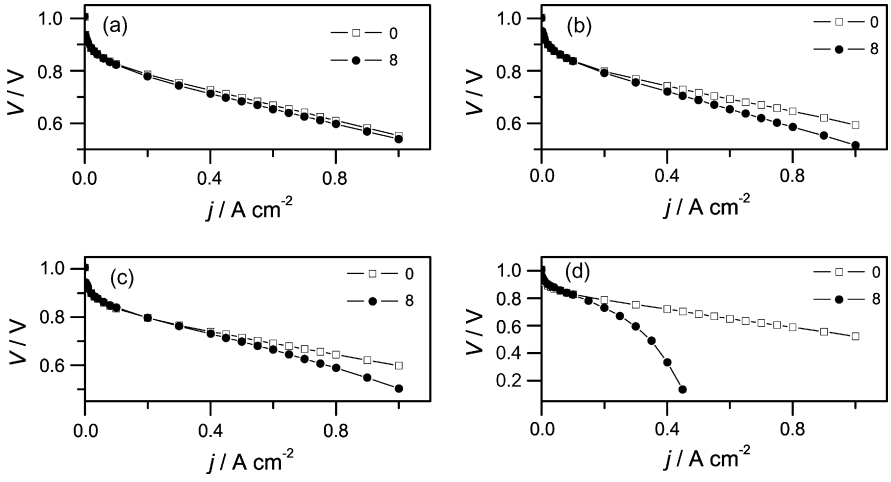

Fig. 1. Performance loss after 8 cycles of freeze at −10 °C for 0.03 MPa H_2/O_2 PEM fuel cells with different residual water amount: (a) C1; (b) C2; (c) C3; (d) C4.

Table 2
The kinetic parameters for 0.03 MPa H_2/O_2 fuel cells before and after frozen at −10 °C

Samples	E_0 (V)	b (mV decade^{-1})	R (Ω cm^2)	$V_{10\,mA}$ (V)
C1				
0	0.9608	72.1	0.23	0.937
8	0.9623	72.4	0.27	0.935
C2				
0	0.9748	74.3	0.22	0.946
8	0.9766	72.3	0.28	0.951
C3				
0	0.9738	72.9	0.23	0.942
8	0.9693	66.4	0.27	0.944
C4				
0	0.9744	78.0	0.24	0.948
8	0.9743	68.2	0.62	0.954

Since the fuel cell performance losses originate from the ohmic polarization, the limited interfacial kinetics, and the limited effective permeability of oxygen in the catalyst layer, the significant performance losses in Fig. 1 can be analyzed. From the EIS general pattern in Fig. 2, the ohmic resistances at different overpotentials obtained from the highest frequency intercept with the real axis are almost the same. The ohmic resistances at 0.1 A cm^{-2} before and after the freezing process are shown as the function of the residual water amount in Fig. 3. The results show that the cell resistance does not change after the 8 freeze/thaw cycles. The performance loss of the cells with different residual water amount does not originate from the increased ohmic resistance. Furthermore, the increased slope of the i–v plots should be owing to the mass transport.

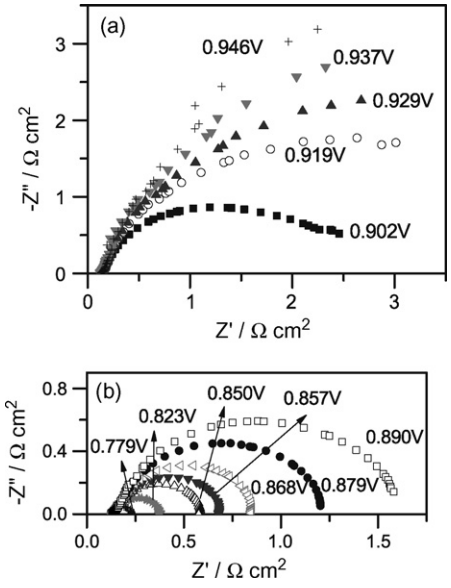

Fig. 2. Typical in situ impedance spectra before freezing at different cathode potentials: (a) from 0.946 to 0.902 V; (b) from 0.890 to 0.779 V.

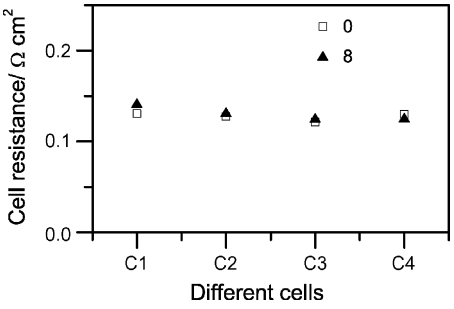

Fig. 3. Cell resistances change at 0.1 A cm^{-2} with different water amount frozen at −10 °C for 8 cycles.

3.3. Change of oxygen transport and charge transfer kinetics

As the resistance obtained from the fitting of the i–v plot includes the cell resistance and mass transport limitation within the CL, the difference of $R - R_{cell}$ ascribes to the mass transport limitation within the CL and the magnitude is denoted as the mass transport resistance. Fig. 4 shows the change of the mass transport resistance at 0.2 A cm^{-2} as function of the water amount. After C1 with 0.9 mg cm^{-2} residual water is frozen at −10 °C for 8 cycles, the mass transport resistance changes a little. For C2 and C3, the changes of the mass transport resistance are almost the same, about 65 mΩ cm^2. Increasing the residual water amount makes the mass transport resistance change significant for C4.

To investigate the change of the charge transfer process before and after the freezing process, the impedance responses at 0.1 and 0.5 A cm^{-2} for each cell are compared. Typical complex Nyquist plots at two current densities before and after the freezing process are shown in Fig. 5. Generally, the diameter of the arc stands for the charge transfer resistance. As in Fig. 2, the impedance characteristic is the diameter of the arc decrease with the overpotential increase. The diameter for the frozen cell is larger than the unfrozen one, which is more significant for the impedance at 0.5 A cm^{-2}. The change of the charge transfer resistances at the two current densities with the residual water amount is shown in Fig. 6. As C4 is not able to run at 0.5 A cm^{-2} after 8 cycles of freeze/thaw, the impedance is not given in Fig. 6b. Increasing the residual water amount in the cell, the change of the charge transfer resistance is more evident. Especially with the largest water amount, the charge transfer resistance even at 0.1 A cm^{-2} greatly increases. The

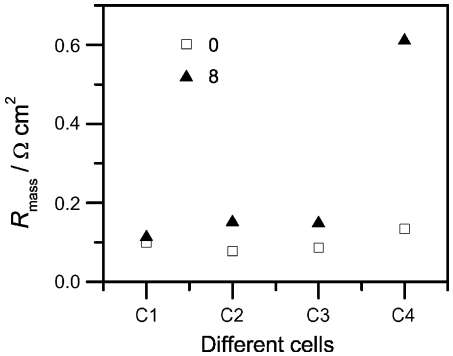

Fig. 4. Change of the mass transport resistance within catalyst layer at 0.2 A cm^{-2} as function of the residual water amount.

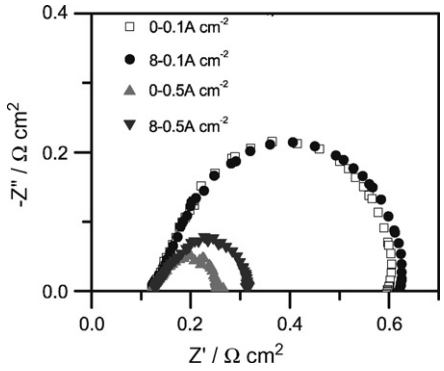

Fig. 5. Typical impedance responses at two current densities before and after the freezing process.

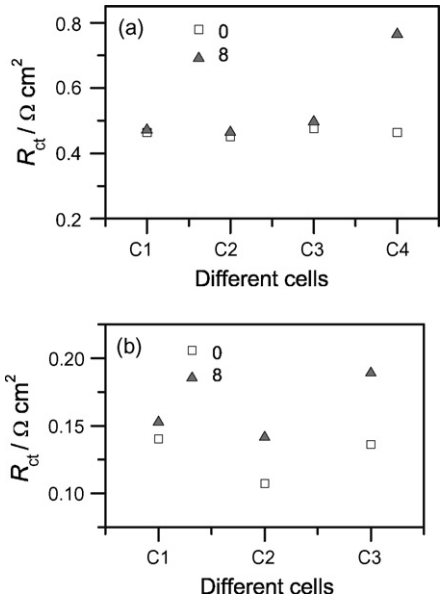

Fig. 6. The change of the charge transfer resistances at two current densities with residual water amount: (a) 0.1 A cm^{-2}; (b) 0.5 A cm^{-2}.

overpotential is small at low current density region and the mass transport contribution to the arc diameter is too small to be neglected. But, C4 mass transport resistance changes a lot after the freezing process as shown in Fig. 4. Whether the change of the charge transport resistance at low current density region contains the contributor from the mass transport is clarified below.

3.4. Residual water correlation

The microstructure of the catalyst layer can be depicted as catalyzed carbon particles flooded with the electrolyte form agglomerates covered with a thin film of electrolyte [19,20]. The reactant gas firstly passes the channels among the agglomerates, diffuses through the ionomer thin film and thereafter in the agglomerates, and then reaches the reaction sites. Considering the porous electrode and the hydrated ionomer, the catalyst layer is able to hold a certain amount of water. The saturation of the CL increases with the residual water amount. But, it is not possible for the generated water to fill the catalyst layer fully. Even in the case of C4, the void pores still exist in the catalyst layer, functioning as the gas channels. That is one of the reasons that the cell is able to run with a specific performance and does not shut down during the process of obtaining the residual water. However, it is most possibly that some of the generated water resides in the pores among agglomerates and does not block the pores, which is shown in Fig. 7a. The residual water fills the pores following the sequence of small hydrophilic pores, large hydrophilic pores, large hydrophobic pores and small hydrophobic pores. With the increase of the residual water amount or the saturation of the CL, the hydrophobic pores will likely be included in the pores among the agglomerates which are filled by the residual water. Once the water freezes, the volume expansion makes the two blocks of ice contact, enlarges the pores among agglomerates and thus compresses the pores in agglomerates. This effect becomes more evident with the cycles increase, as shown in Fig. 7b. The fact that the number of small pores (<25 nm) decreased while the number of big pores (>25 nm) increased [12] supports the changed agglomerates. The pores in agglomerates are more or less compressed, and thus oxygen diffusion within the agglomerates becomes a little more difficult. The generated water can also reside in the pores in the agglomerates. The volume expansion caused by ice formation is much smaller compared with that happens in the pores among the agglomerates. This can be verified by the results from the thin film-flooded agglomerate model. Furthermore, the compressing effect makes the number of the TPBs decrease. The induced

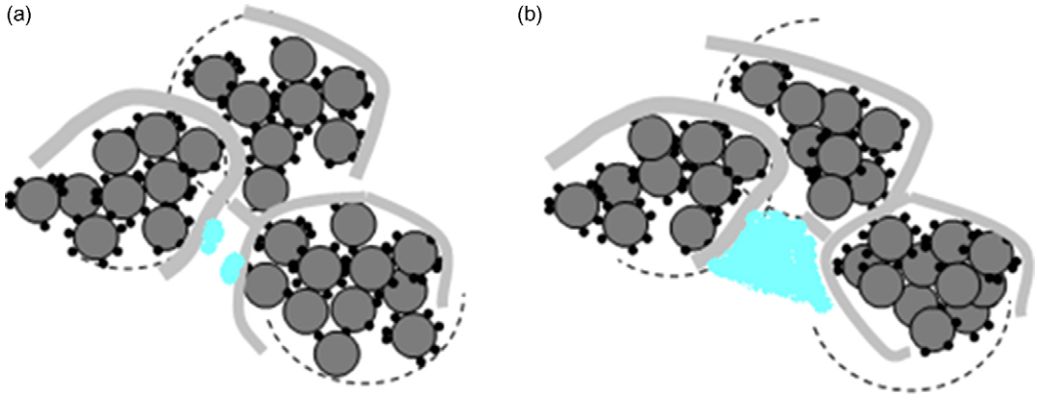

Fig. 7. Schematic thin film-flooded agglomerates after freeze/thaw cycles: (a) initial one; (b) after freeze.

decay of cell performance is irreversible and can be called "irreversible performance loss". Once the ice melts, a thin water film will be formed and block the pore among agglomerates (Fig. 7b). The performance decay induced by this effect is "reversible performance loss". When the residual water amount in the catalyst layer is too small to form a continuous water film, this kind of performance decay does not appear, i.e. C1–C3.

Therefore, the thin film-flooded agglomerate model is applied to analyze the impedance data. The model has been successful in explaining the gas diffusion electrodes behavior. When the diffusion in the agglomerates is the control step of the reaction kinetics, plots of $\log(R_{ct}^{-1})$ as a function of electrode potential must present a double Tafel slope, with respect to the value observed when the charge transfer resistance is the rate determining step [15,18–20]. As seen from the impedance spectra presented in Fig. 2, there is only one loop in the low overpotentials region. In such cases, the charge transfer resistance R_{ct} is associated with the charge transfer process at the catalyst/electrolyte interfaces, and may contain contributions from the mass transport process within the catalyst layer. To investigate the freeze effect at subzero temperature, the cathode potential was plotted as a function of $\log(R_{ct}^{-1})$ for the four cells, as shown in Fig. 8. Based on Eq. (3), the equation $V_{cath} = E_{cell} - b \log i$ can be obtained by iR-crorrected cell voltage. The R_{ct} and the current density in the low overpotentials region have the relation of $R_{ct} = RT/nFi$ [16,21]. Rearranging the equation, then we have

$$V_{cath} = b \log R_{ct} + C \quad (5)$$

Table 3
Tafel slopes in the low current region and high current region before and after the freezing process

Tafel slopes	C1	C2	C3	C4
Low current region				
b_0 (mV decade^{-1})	60.2	65.2	65.5	61.0
b_8 (mV decade^{-1})	63.4	62.1	66.2	62.5
High current region				
b_0 (mV decade^{-1})	125.4	115.2	129.8	157.1
b_8 (mV decade^{-1})	141.4	178.0	212.2	–

By linear-fitting at the low current region, the Tafel slope in this region can be obtained and is summarized in Table 3. b_0 and b_8 stand for the Tafel slope before and after the 8 freeze/thaw cycles. It can be seen that in the low current density region the overpotential dependence arc reflects a pure kinetic control, and the Tafel slopes in this region are almost 63 mV decade^{-1} for the four cells before and after the freezing process. It indicates that the ORR mechanism is the same for the frozen and unfrozen cells. The Tafel slopes obtained by this method are all less than those by fitting the polarization plots. It is reasonable for that the fitting region in the latter situation usually includes mass diffusion effects within the catalyst layer. At the high current density region, the Tafel slopes of the four cells all become steeper. It suggests that there is an agglomerate diffusion effect within the CL for all cells. The second Tafel slope increases after the freezing process especially for the cells with large residual water amount. The Tafel slopes in the high current density before and after the freezing process are also summarized in Table 3.

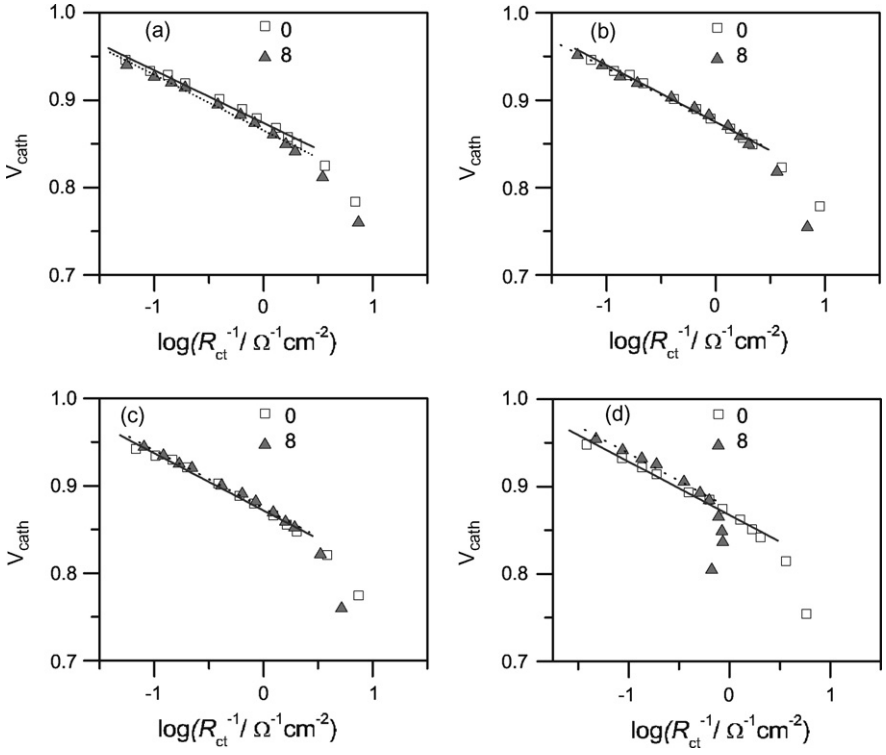

Fig. 8. The plots of $\log(R_{ct}^{-1})$ as function of cathode potential for the four cells experiencing with different residual water amount frozen at −10 °C: (a) C1; (b) C2; (c) C3; (d) C4.

The increased Tafel slopes after the freezing process suggest that the pores in agglomerates have been compressed and thus the agglomerate diffusion effect is more evident. It also indicates that the volume expansion due to water freezing in the pores in the agglomerates can be neglected compared with that occurs in the pores among the agglomerates. As a result, the agglomerates change as in Fig. 7b after 8 freeze/thaw cycles. The increase of the residual water amount makes the CL more saturated, which brings not only the evident agglomerate diffusion effect but also the thin film diffusion effect. After the 8 freeze/thaw cycles, there is a more evident slope change for C4 with the largest water amount as shown in Fig. 8d. The value of $\log(R_{ct}^{-1})$ does not increases linearly with the overpotential and the turn point appears, which reflects the obvious thin film diffusion effect. As a result, the R of C4 in Table 2 increases from 0.24 to 0.62 $\Omega\,cm^2$ and the mass transport resistance within the catalyst layer increases (Fig. 4). This effect is caused by the thin water film of ice melting.

4. Conclusion

By analyzing the EIS results, the ohmic resistance did not change for the cells frozen with the four different residual water amounts. The change of the charge transfer resistance depended on the residual water amount, while the mass transport resistance of the cell with the largest residual water amount increased significantly even at small current density region. Based on the thin film-flooded agglomerate model, the potential-dependence impedance suggested that the mechanism of the oxygen reduction reaction did not change after the cells experienced subzero temperature. The water freezing in the pores among agglomerates compressed the pores in agglomerates, induced agglomerates diffusion effects, and thus resulted in irreversible performance loss. When the amount of the water resided in the pores among agglomerates was enough to form a continuous thin water film, the evident thin film diffusion effect was found. It was predicted that the performance decay induced by this effect was reversible performance loss.

Acknowledgements

This work was financially supported by the National High Technology Research and Development Program of China (863 Program, no. 2005AA501660) and the National Natural Science Foundations of China (nos. 20206030, and 20636060). Kikusui Electronics Corp. is gratefully acknowledged.

References

[1] S. Ge, C.-Y. Wang, Electrochem. Solid State Lett. 9 (2006) A499.
[2] L. Mao, C.-Y. Wang, J. Electrochem. Soc. 154 (2007) B139.
[3] K. Tajiri, Y. Tabuchi, C.-Y. Wang, J. Electrochem. Soc. 154 (2007) B147.
[4] L. Mao, C.-Y. Wang, Y. Tabuchi, J. Electrochem. Soc. 154 (2007) B341.
[5] S. Ge, C.-Y. Wang, Electrochim. Acta 52 (2007) 4825.
[6] M. Oszcipok, D. Riemann, U. Kronenwett, et al., J. Power Sources 145 (2005) 407.
[7] J. St-Pierre, J. Roberts, K. Colbow, et al., J. N. Mater. Electrochem. Syst. 8 (2005) 163.
[8] Q. Guo, Z. Qi, J. Power Sources 160 (2006) 1269.
[9] J. Hou, H. Yu, S. Zhang, et al., J. Power Sources 162 (2006) 513.
[10] M.S. Wilson, J.A. Valerio, S. Gottesfeld, Electrochim. Acta 40 (1995) 355.
[11] R. Mukundan, S.Y. Kim, F. Garzon, B. Pivovar, ECS Trans. 1 (2005) 403.
[12] E.A. Cho, J.-J. Ko, H.-Y. Ha, et al., J. Electrochem. Soc. 150 (2003) A1667.
[13] T.E. Spriger, T.A. Zawodzinski, M.S. Wilson, S. Gottesfeld, J. Electrochem. Soc. 143 (1996) 587.
[14] V.A. Paganin, C.L.F. Oliveira, E.A. Ticianelli, et al., Electrochim. Acta 43 (1998) 3761.
[15] M. Ciureanu, R. Roberge, J. Phys. Chem. B 105 (2001) 3531.
[16] Z. Xie, S. Holdcroft, J. Electroanal. Chem. 568 (2004) 247.
[17] J. Hou, H. Yu, B. Yi, et al., Electrochem. Solid State Lett. 10 (2007).
[18] S.L.A. da Silva, E.A. Ticinanelli, J. Electroanal. Chem. 391 (1995) 101.
[19] T.E. Springer, I.D. Raistrick, J. Electrochem. Soc. 136 (1989) 1594.
[20] I.D. Raistrick, Electrochim. Acta 25 (1990) 1579.
[21] A. Parthasarathy, B. Dave, S. Srinivasan, A.J. Appleby, et al., J. Electrochem. Soc. 139 (1992) 1634.